Importance of Shattering Fragmentation in the Surface-Induced Dissociation of Protonated Octaglycine

Kyoyeon Park,[a] Bipasha Deb,[b] Kihyung Song,[c] and William L. Hase[a]
[a] Department of Chemistry and Biochemistry, Texas Tech University, Lubbock, Texas, USA
[b] Department of Chemistry and Biochemistry, University of Notre Dame, Note Dame, Indiana, USA
[c] Department of Chemistry, Korea National University of Education, Chungbuk, Korea

A QM + MM direct chemical dynamics simulation was performed to study collisions of protonated octaglycine, gly_8-H^+, with the diamond {111} surface at an initial collision energy E_i of 100 eV and incident angle θ_i of 0° and 45°. The semiempirical model AM1 was used for the gly_8-H^+ intramolecular potential, so that its fragmentation could be studied. Shattering dominates gly_8-H^+ fragmentation at θ_i = 0°, with 78% of the ions dissociating in this way. At θ_i = 45° shattering is much less important. For θ_i = 0° there are 304 different pathways, many related by their backbone cleavage patterns. For the θ_i = 0° fragmentations, 59% resulted from both a-x and b-y cleavages, while for θ_i = 45° 70% of the fragmentations occurred with only a-x cleavage. For θ_i = 0°, the average percentage energy transfers to the internal degrees of freedom of the ion and the surface, and the energy remaining in ion translation are 45%, 26%, and 29%. For 45° these percentages are 26%, 12%, and 62%. The percentage energy-transfer to ΔE_{int} for θ_i = 0° is larger than that reported in previous experiments for collisions of des-Arg^1-bradykinin with a diamond surface at the same θ_i. This difference is discussed in terms of differences between the model diamond surface used in the simulations and the diamond surface prepared for the experiments. (J Am Soc Mass Spectrom 2009, 20, 939–948) © 2009 American Society for Mass Spectrometry

Surface-induced dissociation (SID) is a type of inelastic scattering, which has been studied in great detail and was first introduced by Cooks and coworkers [1] in the 1980s to study the fragmentation of peptide ions. In SID, a fraction of the ion's kinetic energy is converted into vibrational excitation resulting in its dissociation. The efficiency of this translational to vibrational energy-transfer strongly depends on the properties of the surface [2–5]. SID occurs via two mechanisms known as non-shattering and shattering [6]. The former is based on the traditional Rice-Ramsperger-Kassel-Marcus (RRKM) [7] model in which the peptide ion is activated by its collision with the surface, and then dissociates by intramolecular vibrational energy redistribution (IVR) after rebounding off the surface. The latter mechanism, shattering, involves fragmentation of the ion as it collides with the surface.

Both chemical dynamics simulations [6, 8–10] and experiments [11–13] have identified shattering as an important mechanism for peptide ion fragmentation. Shattering occurs rapidly, i.e., within $\sim 10^{-14}$–10^{-13} s, as the projectile ion collides with the surface. Thus, there is insufficient time for complete IVR to occur and the unimolecular dynamics of shattering is not in accord with the statistical IVR assumption of RRKM theory. As a result, the dissociation pathways with the lowest potential energy barriers, and predicted to be dominant by RRKM theory, may be relatively unimportant or not observed [10]. Shattering leads to many different dissociation channels [14] and it has been proposed that shattering dissociation depends on the likelihood that the ion is oriented in a proper manner during its interaction with the surface to directly lead the ion to a dissociative transition-state [14]. The formation of an extensive number of different product ions in shattering is beneficial for determining the projectile's primary structure [12, 13].

In chemical dynamics simulations of SID, shattering has been observed for both protonated glycine [6, 10] and diglycine, [9] i.e., gly-H^+ and gly_2-H^+. Experimentally, shattering has also been observed for the larger peptide ion protonated bradykinin [11]. Similar fragmentation dynamics for different size peptide ions is in accord with the observation, both experimentally [15, 16] and computationally [17, 18], that the energy-transfer dynamics are nearly independent of the peptide ion

Address reprint requests to Dr. W. L. Hase, Department of Chemistry and Biochemistry, Texas Tech University, Lubbock, TX 79409, USA. E-mail: bill.hase@ttu.edu

1044-0305/09/$32.00
doi:10.1016/j.jasms.2009.02.028

Published online March 4, 2009
Received December 2, 2008
Revised February 25, 2009
Accepted February 25, 2009

size. The percentage energy-transfer to the ion's internal degrees of freedom is at most only weakly dependent on the ion's size and structure [14].

For the work presented here, a QM + MM direct dynamics simulation [19, 20] was performed, using the AM1 semiempirical electronic structure theory, to model SID of protonated octaglycine, gly_8-H^+, in collisions with the diamond {111} surface. Of particular interest is to determine whether shattering is important for this ion as found in the previous simulations for gly-H^+ and gly_2-H^+. The methodology and results of this study are presented in the following. The results are also compared with experimental findings [11–13] as well as previous work on peptide ions of varied size [15–18].

Computational Procedure

Potential Energy Function

A QM + MM direct dynamics simulation [19, 20] was performed to study SID in collisions of gly_8-H^+ with the diamond {111} surface. The complete potential energy function used for the simulation is given by:

$$V = V_{ion} + V_{surf} + V_{ion\text{-}surface} \quad (1)$$

where V_{ion} is the ion's intramolecular potential, V_{surf} the potential for the surface, and $V_{ion\text{-}surface}$ the intermolecular potential between the ion and the surface. In the work presented here V_{ion} and its derivatives are obtained directly from a quantum mechanical (QM) theory, and V_{surf} and $V_{ion\text{-}surface}$ are represented by molecular mechanical (MM) analytic functions. As a result, the simulation is referred to as QM + MM direct dynamics [20].

The semiempirical QM theory, AM1, was used to represent the intramolecular potential for gly_8-H^+. AM1 theory provides a quite good representation of potential energy barriers for protonated glycine dissociation [6]. Though it is more computationally expensive, it is superior to the molecular mechanical (MM) model AMBER, [21] which only considers harmonic-like nuclear potentials and, thus, does not describe dissociation pathways for peptide ions. *Ab initio* QM methods may also be used for direct dynamics simulations, [19, 20] but they are extremely "expensive" in terms of computational resources. Though an ab initio method was used for the small peptide ion gly-H^+,[10] they are computationally impractical for the much larger ion gly_8-H^+. For the work presented here, the much less expensive QM method AM1 was used. Previous work has shown that nearly the same energy-transfer efficiencies are obtained when either AMBER, AM1, or MP2/6-31G* are used to represent the peptide ion's intramolecular potential V_{ion} [6, 9, 10, 14]. In chemical dynamics simulations of gly-H^+ SID, the same shattering probabilities are obtained when using either AM1 or MP2/6-316* for V_{ion} [10, 14].

The MM potential energy function for the diamond surface consists of harmonic stretches and bends, with force constants chosen to fit the diamond phonon spectrum [22]. To represent the peptide-surface intermolecular potential a MM analytic function was used, comprised of two-body potential functions of the form

$$V_{XY} = A_{XY} \exp(-B_{XY}\, r_{ij}) + C_{XY}/r_{ij}^6 \quad (2)$$

where X and Y represent the C, H, N and O atoms of the peptide and C and H atoms of diamond, respectively. Parameters for these potentials were determined using CH_4, NH_4^+, H_2CO, NH_3 and H_2O as models representing different types of atoms and functional groups of the peptide ion [17]. This potential accurately describes the short-range, repulsive interactions which determine the collisional energy-transfer, but not the long-range intermolecular potential. The latter describes the attractive interaction of the peptide ion with the surface and is necessary to model soft-landing experiments [23, 24] in which the ion binds to the surface. Work has been done to develop these potentials [25].

Trajectory Simulations

Direct dynamics simulations were performed, with a software package consisting of VENUS [26] and Gaussian, [27] to model collisions of gly_8-H^+ with the diamond {111} surface. The simulations were performed for a collisional energy of 100 eV and incident angles of

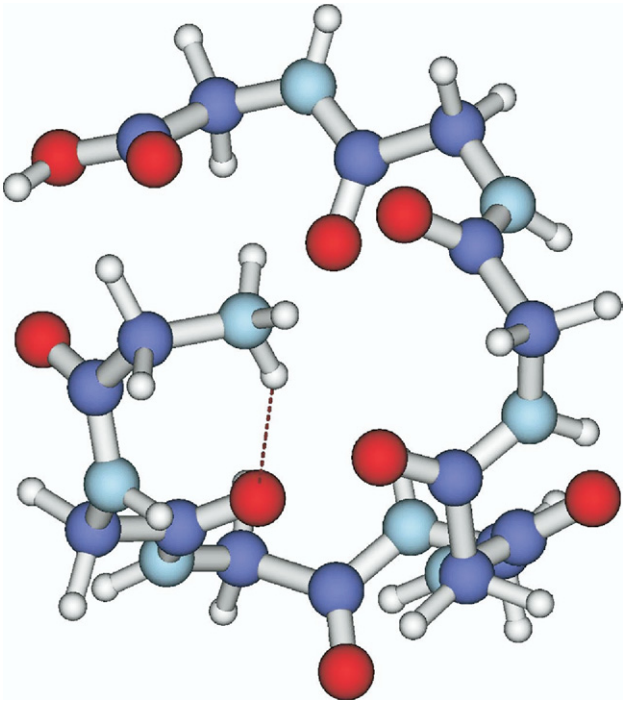

Figure 1. The folded structure for gly_8-H^+ used to choose initial conditions for the chemical dynamics simulations. The light blue, dark blue, red, and white balls represent nitrogen, carbon, oxygen, and hydrogen atoms, respectively.

0° (normal to the surface) and 45°. Initial conditions for the simulations were chosen for gly_8-H^+ in the folded structure shown in Figure 1. This structure was determined by first performing a 300 K molecular dynamics simulation for gly_8-H^+ based on the MM2 molecular mechanical potential [28]. Gly_8-H^+ equilibrated to a folded structure, which was then optimized to give the equilibrium structure in Figure 1. Initial conditions for the vibrational and rotational degrees of freedom of the peptide, representing a 300 K Boltzmann distribution, were chosen using the quasi-classical normal mode method [29]. The peptide ion was randomly rotated about its center of mass and directed at a randomly chosen impact site on the surface. The azimuthal angle, for collision of the projectile ion with the surface, was chosen randomly between 0 and 2π to simulate collisions with different domains of growth on the surface [30].

The diamond surface, used for the simulations, consisted of a hydrogen terminated top layer and eight layers of carbon atoms with a total number of carbon atoms equal to 6950 and a thickness of ~13 Å. The surface initial conditions were chosen by assigning velocities to the surface atoms, sampled from a Maxwell Boltzmann distribution at 300 K. The velocities were then scaled [31] such that the temperature was that for a 300 K Boltzmann distribution by equilibrating the surface for 2 ps of molecular dynamics. The structure thus obtained was then used as the initial structure for an equilibration run at the beginning of each trajectory.

A sixth order symplectic integrator [32] was used to integrate the classical equations of motion with an integration step size of 2 fs. The trajectories were allowed to run for a maximum total time of 4 ps. For the collision energy of 100 eV, a total of 377 and 103 trajectories were computed, respectively, for the incident angles of 0° and 45°. The initial separation between the center of mass of gly_8-H^+ and the top of the surface was set at 25 Å at the start of each trajectory. The trajectory was terminated if this separation exceeded 30 Å. The trajectories were calculated on a heterogeneous cluster consisting of different single core processors. On average it took ~1 and 2/3 days to integrate a trajectory for 4 ps on one of these processors using a 2 fs time step.

The initial 100 eV translational energy of gly_8-H^+ may be transferred to the surface as well as to the ion's internal modes and the energy conservation relationship is given by:

$$E_i = \Delta E_{int} + \Delta E_{surf} + E_f \quad (3)$$

where ΔE_{int} and ΔE_{surf} are the energy transfers to the vibrational degrees of freedom of gly_8-H^+ and to the vibrational modes of the surface, respectively, and E_f is the energy remaining in the ion's translational motion. The efficiencies of energy-transfer to ΔE_{int} and ΔE_{surf} were determined for each trajectory. Also investigated was the fragmentation mechanism, i.e., dissociation following IVR or shattering.

Simulation Results

The trajectories were analyzed for (1) the percentage energy transfers to ΔE_{int}, ΔE_{surf}, and E_f, and their distributions; (2) the fraction which fragmented during their 4 ps numerical integrations; (3) the type of fragmentation, i.e., dissociation following IVR or shattering; and (4) the backbone cleavage patterns for the fragmentations. Of particular interest is the dependence of these SID dynamics on the incident angle, i.e., either 0° (normal to the surface) or 45°.

Energy Transfer Efficiencies

The efficiencies of energy-transfer to the surface and to the projectile's internal degrees of freedom are important attributes of SID. The probability and mechanism for projectile fragmentation depend on the transfer of the collision energy to the projectile's vibrational degrees of freedom. The average percentages for energy-transfer to the projectile's internal degrees of freedom, ΔE_{int}, and to the surface, ΔE_{surf}, and of the energy remaining in projectile translation, E_f, are listed in Table 1. Changing the incident angle, from a perpendicular collision, $\theta_i = 0°$, to 45° reduces the energy-transfer to ΔE_{int} and ΔE_{surf} and retains more energy in projectile translation. For $\theta_i = 0°$ nearly fifty per-cent, i.e., 0.45, of the collision energy E_i is transferred to ΔE_{int}. The distributions of energy-transfer to ΔE_{int}, ΔE_{surf}, and E_f, for the $\theta_i = 0°$ collisions, are shown in Figure 2. Their forms are similar to those found previously [6, 9, 10, 14, 17, 18] for simulations of the smaller gly_n-H^+ peptide ions and for the current study with $\theta_i = 45°$.

Fragmentation Probability and Mechanism

The fragmentation probability and mechanism depend on the incident angle, θ_i. Of the 377 trajectories calculated for $\theta_i = 0°$, 351 (i.e., 0.93) of the gly_8-H^+ ions fragmented within the 4 ps time of the trajectory integration. For the $\theta_i = 45°$ trajectories, 33/103 = 0.32 dissociated during the trajectory integration. The larger fragmentation at $\theta_i = 0°$ is consistent with the greater transfer to ΔE_{int} for this incident angle. It took the ion 395 fs to hit the surface and, thus, the internal motion of the excited ion was followed for a maximum time of 3.6 ps. For each trajectory, at both θ_i of 0° and 45°, the internal energy-transfer to the peptide ion, ΔE_{int}, is

Table 1. Percentage energy transfers for gly_8-H^+ + diamond {111} collisions[a]

θ_i (°)	ΔE_{int}	ΔE_{surf}	E_f
0[b]	0.45	0.26	0.29
45[c]	0.26	0.12	0.62

[a]The collision energy is 100 eV.
[b]The standard deviations of the mean for these percentages is ± 0.01.
[c]The standard deviation of the mean for these percentages range from 0.005 for E_f to 0.02 for ΔE_{surf}.

greater than the lowest energy potential energy barrier for the ion's fragmentation [6] and, thus, if longer times are considered each ion is expected to dissociate.

For the calculations at $\theta_i = 0°$, a careful analysis was done to determine the number of fragments for each gly_8-H^+ ion that fragmented. This number varies between 2 and 16, and a scatter plot is given in Figure 3 of the number if fragments versus ΔE_{int}. There is a tendency for the number of fragments to increase with increase in ΔE_{int}, but it is not particularly strong. Some of the fragments may contain sufficient internal energy to undergo unimolecular dissociation if the trajectories were followed for more than 4 ps. This would increase the number of fragments for the initially fragmenting gly_8-H^+ ion.

Shattering occurs as the projectile ion collides with the surface and the fraction of trajectories which shatter will not increase with longer integration times. Of the trajectories calculated at $\theta_i = 0°$, 293/377 = 0.78 shatter. At $\theta_i = 45°$, this fraction is much lower and 23/103 = 0.22. Shattering dominates the fragmentation at $\theta_i = 0°$ and a feature of shattering are the many different fragmentation pathways and the resulting many different fragment ions. A representative trajectory illustrating shattering fragmentation is shown in Figure 4. A plot of the m/e ratios for the different product ions, versus their populations, is given in Figure 5 for the $\theta_i = 0°$ calculations. The ten most dominant m/e peaks in decreasing importance, with their relative populations, are 30 (1.00), 102 (0.88), 159 (0.66), 258 (0.41), 45 (0.39), 58 (0.39), 144 (0.39), 201 (0.37), 87 (0.34), and 216 (0.34), respectively. For some of these peaks, there is only one ion, but for others there are more than one. The ions in the respective peaks, including the populations of multiple ions within the peaks, are as follows: $NH_2CH_2^+$; $CONHCH_2CO_2H^+$; $[CONHCH_2]_2CO_2H^+$; $NH_2[CH_2CONH]_4CH_2^+$; CO_2H^+; $CHONHCH_2^+$ (0.81), $NH2CH2CO^+$ (0.19); $NH_2[CH_2CONH]_2CH_2^+$ (0.94), $COCH_2NHCOCH_2CO_2H+$ (0.06); $NH_2[CH_2CONH]_3CH_2^+$; $NH_2CH_2CONHCH_2^+$; and $[CONHCH_2]_3CO_2H^+$. The ion populations versus m/e are plotted in Figure 5 for the calculations at $\theta_i = 45°$.

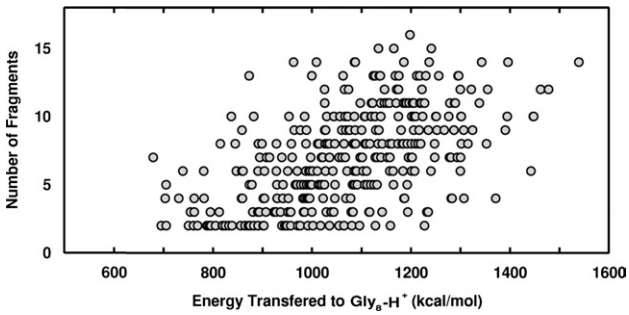

Figure 3. Scatter plot of the number of fragments versus the energy transferred to the internal degrees of freedom of gly_8-H^+, for each of these ions that fragmented at $\theta_i = 0°$ and $E_i = 100$ eV.

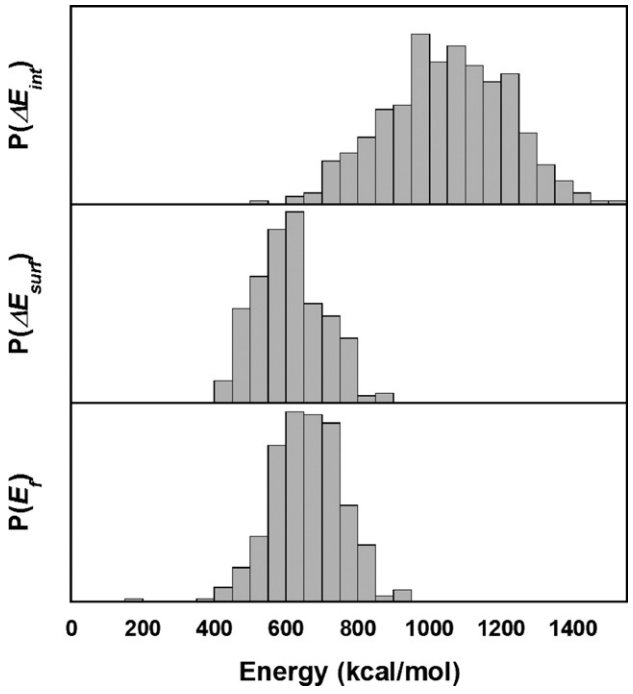

Figure 2. Distributions of energy-transfer to the gly_8-H^+ ions' internal degrees of freedom (ΔE_{int}) of energy-transfer to the surface (ΔE_{surf}), and of the recoiling ions' translational energy as a result of collisions with the diamond {111}surface at an initial collision energy of 100 eV (2306 kcal/mol) and θ_i of 0° and normal to the surface.

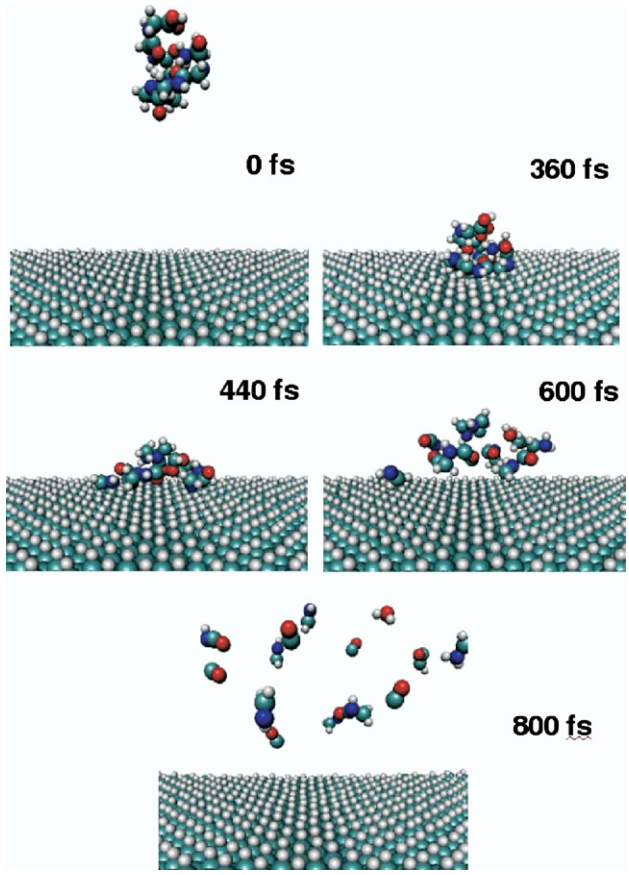

Figure 4. Representative trajectory illustrating scattering fragmentation of gly_8-H^+. The fragments at 800 fs are H_2O, 6 CO, 6 $NHCH_2$, $NH_2CH_2^+$, CONH, and $COCH_2$.

Here the number of trajectories and number of fragmentations are much smaller than at $\theta_i = 0°$. The five most dominant m/e peaks are 372 (1.00), 315 (1.00), 387 (0.75), 258 (0.75), and 201 (0.75), respectively. The ions, in the respective peaks, are: $NH_2[CH_2CONH]_6CH_2^+$; $NH_2[CH_2CONH]_5CH_2^+$; $NH_2[CH_2CONH]_4CH_2^+$; $NH_2[CH_2CONH]_3CH_2^+$; and $[CONHCH_2]_6CO_2H^+$. There are both similarities and differences with the $\theta_i = 0°$ results.

As discussed above, the internal motion of each excited ion was followed for a maximum time of only 3.6 ps. For each trajectory, at both θ_i of 0° and 45°, the internal energy-transfer to the peptide ion, ΔE_{int}, is greater than the lowest energy potential energy barrier for the ion's fragmentation [6] and, thus, if longer times are considered each ion is expected to dissociate and form additional fragments. Also, some of the fragments found in the current study may contain sufficient internal energy to undergo unimolecular dissociation if the trajectories were followed for a longer period. Thus, some of the ions identified as products in Figure 5 may dissociate. This would further increase the number of fragment ions. As a result the ion yields in Figure 5 may not be directly compared with experiment [33].

To compare with experiment, the gly_8-H^+ ions and fragment ions must be properly accounted for, which have sufficient energy to dissociate but are undissociated when the trajectories are halted at 4 ps. This may be done if these ions are assumed to have undergone efficient IVR, so that RRKM theory may be used to calculate the rate constants for their unimolecular pathways and, thus, the yield of their fragmentation products. In addition to knowing the internal energy of the undissociated gly_8-H^+ molecules, this will require knowing the internal energy of the fragment ions which have sufficient energy to dissociate. Furthermore, the transition-state vibrational frequencies and dissociation barriers are required for all of the dissociation pathways. Such an analysis will be a substantial effort, but necessary to make a direct comparison between simulation and experiment.

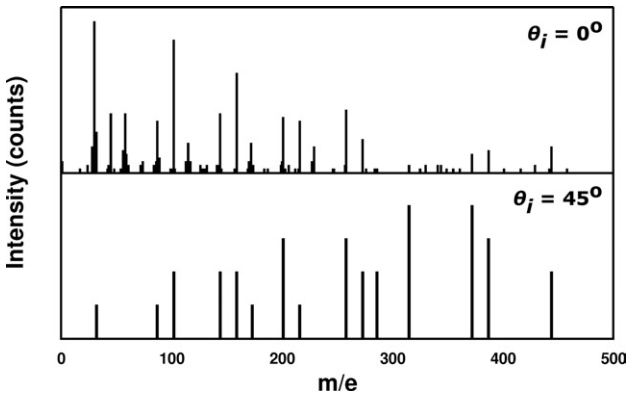

Figure 5. Population of fragment ions versus their m/e ratios for gly_8-H^+ + diamond {111} fragmentation at $E_i = 100$ eV for $\theta_i = 0°$ (normal to surface) and $\theta_i = 45°$. Fragmentation is for 3.6 ps of internal motion of the excited gly_8-H^+ ions. The peak for gly_8-H^+ is not included.

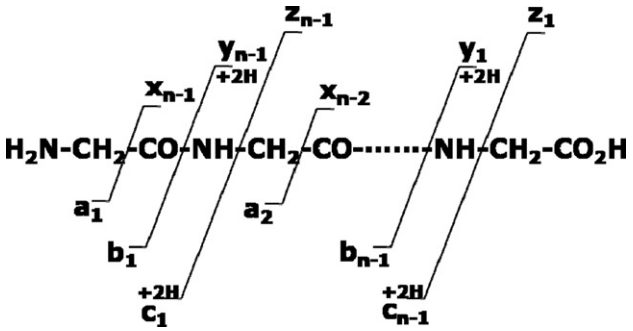

Figure 6. Nomenclature for a protonated peptide ion's fragments and possible backbone cleavage sites.

Backbone Cleavage Patterns

In this study, the same nomenclature was used for fragment ions (see Figure 6) as in typical mass spectrometry studies [33]. The observed types of backbone cleavages and their populations are listed in Table 2. The most dominant cleavage sites were a-x and b-y for $\theta_i = 0°$, and a-x for $\theta_i = 45°$. C-z type cleavage was also observed in ~20% of the trajectories. However, this is not an independent cleavage and occurred typically with a-x and b-y type cleavages. With $\theta_i = 0°$, multiple backbone cleavages were observed for ~82% of the trajectories, consisting of a-x and b-y, or a-x, b-y, and c-z. However, for $\theta_i = 45°$, only a single a-x type cleavage was dominant.

Most of the backbone cleavages occurred via shattering for both incident angles. When gly_8-H^+ collides with the surface, its structure is highly distorted, causing a high strain on the backbone and leading to shattering fragmentation (Figure 4). For $\theta_i = 0°$ almost all of the charged ions (Figure 5) are formed by shattering. Shattering is also important for $\theta_i = 45°$, but here 18% of the principal charged ions are formed by nonshattering processes.

For the $\theta_i = 0°$ collisions, 2 to 16 fragments were formed for each trajectory and fragmentation occurred via 304 different reaction channels, related by their backbone cleavages. Many different neutral molecules were formed, with CO and $NHCH_2$ the most prevalent.

Table 2. Backbone cleavage patterns for gly_8-H^+ + diamond {111} SID[a]

	Number of trajectories[b]	
Backbone cleavage patterns	$\theta_i = 0°$	$\theta_i = 45°$
a-x	55 (15.7)	23 (69.7)
b-y	1 (0.3)	0 (0.0)
a-x and b-y	208 (59.3)	9 (27.3)
a-x, b-y and c-z	69 (19.6)	1 (3.0)
a-x with NH_3 loss	5 (1.4)	0 (0.0)
a-x and b-y with NH_3 loss	12 (3.4)	0 (0.0)
NH_3 loss	1 (0.3)	0 (0.0)
	Total: 351	Total: 33

[a]The collision energy is 100 eV.
[b]The percentage of the cleavage pattern is given in parentheses.

Of the 377 trajectories calculated with $\theta_i = 0°$, 277 trajectories (79%) formed either CO or $NHCH_2$, of which 251 trajectories (72%) formed both CO and $NHCH_2$. In contrast to the previous simulations of small peptides, [6, 9, 10] CO and $NHCH_2$ formation followed a backbone cleavage, which occurred during or immediately after shattering. Approximately 9% of the trajectories formed NH_3, which did not occur by shattering, but later after the ion had rebounded off the surface. This is understandable, because the NH_3 -group (N-terminal site) is coiled inside the folded structure and not exposed during the surface impact, which is the case for small peptide ions. Of the $\theta_i = 0°$ trajectories, only 4% had H^+ or H_2 loss, 2% H_2O loss, and 2% HCN loss. NH_3, H_2, and H_2O were formed after gly_8-H^+ collided with the surface and dissociated by an IVR mechanism.

The fragmentation dynamics is dramatically changed for $\theta_i = 45°$. Shattering still dominates, but the number of fragments is much less than for $\theta_i = 0°$. Of the 33 dissociating trajectories, 23 (70%) formed two fragments consisting of a a_n or x_n type ion. For the remaining 10 dissociating trajectories, 2 formed 3 fragments, 7 formed 4 fragments, and only 1 formed a large number of fragments, i.e., 8. The 9 trajectories fragmenting, via a-x and b-y type backbone cleavage, formed either CO or $NHCH_2$. Neither NH_3, H_2, or H_2O were formed from the collisions at $\theta_i = 45°$.

A total of 426 ions were formed from the 351 dissociating trajectories at $\theta_i = 0°$ and, amongst these, there were 135 different kinds of ions. Except for three H^+ and one OH^+, most of the ions resulted from either an a-x or b-y type bond cleavage, or combination of both. Only 13 ions were formed from c-z type bond cleavages. About 20% of the trajectories had c-z type backbone cleavages, but they mainly produced neutral molecules such as $COCH_2$, CONH, and sometimes HCN. The tendency found here, for the a, b, x and y type ions to be the major peaks in the mass spectrum, is the same as for typical MS/MS SID experiments [34].

Rearrangement of Product Fragments

In protonated peptide ion dissociation, reactions in which the atoms of the peptide backbone are rearranged are often important [35–37], and such rearrangement reactions were observed in this study. Most of these rearrangements occurred on or near the surface, after impact, when the structure of the folded peptide ion was highly distorted. Among the 351 dissociating trajectories for $\theta_i = 0°$, 63 gave rearrangement products and 59 of these were shattering events. Thirty of the rearranged products are ions and the remaining 33 neutral. Of the 30 charged rearrangement products, 17 have masses different than those for typical a, b, x, and y fragments, while the remaining 13 have masses typical of product fragments. Hence, the fraction of the rearranged fragments which have unique masses in the spectrum is 17/426 = 0.04, where 426 is the total number of ion fragments for $\theta_i = 0°$.

For the $\theta_i = 0°$ simulations, there are two rearrangement mechanisms for the shattering trajectories. One is intramolecular recombination of fragments, forming a ring type intermediate structure. The other results from various bond cleavages and ensuing fragment recombinations. For the former, the ends of two fragments recombine and form a 5 to 12 membered ring, after backbone breakage occurs by surface impact. These ring structures have masses and sequences consistent with the peptide backbone. Some backbone cleavages, caused by shattering, result in fragments with two reactive end groups (e.g., –NH and $–CH_2$), which are not yet stabilized by mobile protons. These end groups recombine, forming a new $–NH–CH_2-$ bond, before the fragment rebounds off the surface. The dynamics of these ring formations are related to the folded structure of the gly_8-H^+ ion. Immediately after the collision, sites where backbone cleavages have occurred are close to each other and end groups recombine before the fragments are stabilized by mobile protons or intramolecular structural rearrangements.

For the rearrangements resulting from various bond cleavages and ensuing fragment recombination with $\theta_i = 0°$, several different kinds of recombination mechanisms were observed. For one, the a_3 ion first loses its $–CH_2NH_3^+$ end group, i.e.

$$^+NH_3\text{-}CH_2\text{-} + \text{-}CO\text{-}NH\text{-}CH_2\text{-}CO\text{-}NH\text{-}CH_2\text{-}$$

Then the moiety on the right recombines with CO_2H^+, formed by C-terminal C-C bond cleavage to give

$$HO\text{-}CO\text{-}CO\text{-}NH\text{-}CH_2\text{-}CO\text{-}NH\text{-}CH_2^+$$

These events happen rapidly on the 40–80 fs timescale, while the fragments are near the surface. After backbone breakage by shattering, many of the fragments rebound quickly from the surface, but some of the more reactive fragments recombine before they have time to move far above the surface. Thus, these rearrangement events are happening mostly on the surface, and are highly correlated with the surface impact and shattering fragmentation. A similar kind of rearrangement and isomerization was observed in the previous simulation of gly-H^+ + diamond {111} collisions [10]. For gly-H^+, the major isomerization occurred at the C-terminal site, with the terminal carboxylic acid group isomerizing to geminal diol ($H_3N\text{-}CH_2\text{-}COOH \rightarrow H_2N\text{-}CH_2\text{-}C(OH)_2$). As found for the current study, this isomerization also occurred as the peptide ion impacted the surface.

For the $\theta_i = 45°$ simulations only two trajectories gave rearranged products. One was a rearrangement by recombination of two fragments, and the other resulted from backbone breakage and self-recombination.

Comparison with Previous Simulations

Energy Transfer Efficiencies

For this gly_8-H^+ + diamond {111} simulation at E_i = 100 eV, the percentage energy-transfer to ΔE_{int} increases by a factor of 1.7 in changing θ_i from 45° to 0° and normal to the surface. Such a pronounced effect is not seen in a simulation of gly_2-H^+ collisions with a perfluorinated octanethiol self-assembled monolayer (F-SAM) surface, for E_i in the range of 30–70 eV [38]. For this system, energy-transfer to ΔE_{int} increases by only a factor 1.3 in changing θ_i from 45° to 0°. The different energy-transfer dynamics for diamond and SAM surfaces is important and quite interesting, and discussed in detail in the next section.

The ΔE_{int}, ΔE_{surf}, and E_f energy-transfer percentages for gly_8-H^+ + diamond {111} are compared, in Table 3, with those determined in previous simulations for gly_n-H^+ (n = 1,2,3,5) ions colliding with diamond {111} [6, 9, 10, 17, 18, 39]. A number of important findings are present in this table and discussed in the following.

The energy-transfer efficiencies do not depend on the intramolecular potential used for gly_n-H^+, since the MP2 *ab initio*, AM1 semiempirical, and AMBER empirical potentials give the same results. For a particular gly_n-H^+ ion, the percentage energy-transfer is only weakly dependent on E_i, with a tendency to slightly decrease for the largest E_i. However, the effects on ΔE_{surf} and E_f are substantial, with energy-transfer to the former increasing and to the latter decreasing with increase in E_i. For E_i of 5 and 10 eV, less than 10% of the collision energy is transferred to ΔE_{surf}. Energy-transfer to ΔE_{int} increases with increase in size of the gly_n-H^+ ions. At θ_i = 45°, the percentage energy-transfer to ΔE_{int} is 11% for gly-H^+, but 23% for gly_5-H^+ and 25% for gly_8-H^+. (These percentages are for different E_i and, thus, the comparison is approximate.) A similar effect is seen at θ_i = 0°, where the transfer to ΔE_{int} is 17% for gly-H^+ and 45% for gly_8-H^+. Changing the gly_n-H^+ collision from normal to the surface (θ_i = 0°) to 45° significantly decreases energy-transfer to ΔE_{int} and ΔE_{surf}. For ΔE_{int}, the decrease is ~1.5 and ~1.7 for gly-H^+ at E_i = 70 eV and gly_8-H^+ at E_i = 100 eV, respectively. A similar factor of ~1.5 is seen for gly_2-H^+.

Energy-transfer in collisions of peptide ions with a diamond surface has not been investigated as extensively in experiments as has been done by chemical dynamics simulations. The only ion studied experimentally is the octapeptide des-Arg[1] 1-bradykinin at θ_i = 0° and E_i of 12-58 eV [16]. It would be of interest to experimentally study collisions of different peptide ions with a diamond surface, and over a range of θ_i and E_i. However, as discussed in the next section, the diamond surface used in the experiments is different from the diamond {111} surface used in the simulations, and a

Table 3. Comparison of percentage energy transfers in Gly_n-H^+ + diamond {111} collisions[a]

Ion	E_i (eV)	Potential	ΔE_{int}	ΔE_{surf}	E_f	Ref.
θ_i = 0°						
gly-H^+	70	MP2	17	47	36	[10]
gly_2-H^+	30	AM1	24	27	49	[9]
		AMBER[b]	27	29	44	[39]
	50	AM1	21	37	42	[9]
	70	AM1	20	40	40	[9]
		AMBER	22	41	37	[39]
	100	AM1	17	48	35	[9]
gly_8-H^+	100	AM1	45	27	29	This work
θ_i = 45°						
gly-H^+	70	MP2	11	39	50	[10]
		AM1	12	38	50	[6]
		AMBER	11	37	52	[60]
gly_2-H^+	5	AMBER	16	0	84	[18]
	10	AMBER	17	4	79	[18]
	30	AMBER	16	12	72	[18]
	70	AMBER	13	26	61	[9]
		AM1	15	25	60	[18]
	110	AMBER	13	34	53	[18]
gly_3-H^+	30	AMBER	18	9	73	[17][c]
	70	AMBER	17	21	62	[17]
	110	AMBER	14	29	57	[17]
gly_5-H^+	30	AMBER	23	5	72	[17]
gly_8-H^+	100	AM1	25	12	62	This work

[a]The results are for folded gly_3-H^+ and gly_5-H^+ structures. The uncertainties (i.e., standard deviation of the mean) in the average percentage energy transfers are approximately ±1%.
[b]Collision energy is 35 eV.
[c]For extended gly_3-H^+, and θ_i = 45° and E_i = 30 eV, the percentage energy transfers to ΔE_{int}, ΔE_{surf}, and E_f are nearly the same as those folded gly_3-H^+ and 20, 8, and 80, respectively.

comparison of the experiments and simulations would be uncertain.

Effect of Peptide-H^+ Structure

Previous chemical dynamics simulations [17] for folded and linear structures of gly_3-H^+ and gly_5-H^+ have shown that the SID energy-transfer dynamics are, at most, only weakly dependent on the structure of the peptide ion. However, it has not been shown that the efficiency of shattering in SID is independent of the peptide structure and it would be of interest to investigate this possible effect in future studies. For additional studies of gly_8-H^+ and/or other protonated polypeptide ions, structures and energies could be determined for different potential energy minima and their energy-transfer and fragmentation dynamics studied.

A property $<A>$ of the peptide ion is an average of the value of the property A_i for each of the ion's structures multiplied by the Boltzmann probability P_i of the presence of the structure at temperature T; i.e.,

$$<A> = \Sigma P_i A_i \quad (4)$$

Here A_i includes distributions $f_i(x)$, such as those for collisional energy-transfer in SID. The folded structure used for gly_8-H^+ in the work reported here is the one obtained from a MD simulation in which gly_8-H^+ was equilibrated at 300 K. However, there is interest in studying the dynamics of structures which have lower probabilities of being populated at 300 K. In particular, there is substantial interest in determining whether the dynamics of linear protonated polypeptide ions are substantially different than those for folded gly_8-H^+ studied here. Such linear peptide ions are expected to become low-energy structures, if they have multiple protonation, e.g., one H^+ ion for each amino acid.

Comparison with Previous Experiments

A particularly interesting finding of the current study is the strong dependence of the energy-transfer on the incident angle, θ_i, as shown in Table 1. Such an effect is not seen experimentally in collisions with a surface consisting of large organic molecules or self-assembled monolayers, [40–42] and computationally in collisions with a self assembled monolayer (SAM) [38]. Herman and coworkers [40] studied collisions of ethanol molecular ions, $C_2H_6O^{+\bullet}$, with stainless-steel surfaces covered by a multilayer of hydrogen-containing substances, usually identified as (pump oil) hydrocarbons, and found that the probability of energy-transfer to the ion's internal degrees of freedom, ΔE_{int}, is independent of θ_i in the range of 40° to 80°. They found the same result in collisions of the same ion, $C_2H_6O^{+\bullet}$, with perfluoro (F-SAM), hydrogenated (H-SAM), and -COOH terminated (HOOC-SAM) alkylthiol self-assembled monolayer surfaces for collisions with θ_i in the same range [41, 42]. In simulation of gly_2-H^+ collisions with a perfluorinated octanethiol F-SAM surface [38], the energy-transfer to ΔE_{int} is similar for collisions with θ_i of 0° and 45°. For θ_i = 0°, the percentage transfer to ΔE_{int} changes from 11% to 13% as E_i is increased from 30 eV to 70 eV. For θ_i = 45°, this percentage change is 15% to 17%. The small difference between the results for these two θ_i indicates that energy-transfer to ΔE_{int} is slightly more efficient for collisions not normal to the surface with θ_i = 45°. It is of interest that though the simulated energy-transfer to ΔE_{int}, is not strongly dependent on θ_i, when θ_i is changed from 0° to 45°, there is a significant decrease in the energy-transfer to ΔE_{surf} and a significant increase in the energy remaining in E_f.

In contrast to the above results, the current study shows that energy-transfer to ΔE_{int}, for gly_2-H^+ + diamond {111} collisions at E_i = 100 eV, is substantially more efficient for θ_i of 0° than 45°. The percentage energy-transfer to ΔE_{int} is 1.7 times larger for θ_i = 0° compared with θ_i = 45°. The origin of the different energy-transfer dynamics for the diamond {111} surface compared with the hydrocarbon (pump oil) and SAM surfaces is uncertain, but may be related to the greater roughness and higher corrugation for the latter surfaces [43, 44] compared with the "perfect" diamond {111} surface used in the current study. This may make energy-transfer to the internal degrees of freedom of projectile ions less dependent on the incident angle.

In an experimental study [16], a percentage energy-transfer to ΔE_{int} of 19.2% was determined for collisions of the octapeptide des-Arg^1-bradykinin with a diamond surface. The incident angle was 0° and the same percentage energy-transfer was found for collisions with E_i in the range of 12–58 eV. As part of the work presented here, for the octapeptide gly_8-H^+, a percentage energy-transfer to ΔE_{int} of 45% was found for collisions with the diamond {111} surface for θ_i = 0° and E_i = 100 eV. This percentage is approximately a factor of two larger than that measured for des-Arg^1-bradykinin at the same θ_i = 0° (i.e., normal collisions) and a slightly smaller E_i.

Such different ΔE_{int} energy-transfer efficiencies, both for an octapeptide, is unexpected and requires an understanding. A possible explanation for this difference is the perfectly flat diamond {111} surface used for the simulations compared with the "rough" diamond surface used in the experiments [16, 45]. The diamond surface is grown by "merging" of different nucleation sites and is inherently rough. In addition, the fraction of carbon on the surface which is graphitic is uncertain [46]. Thus, there are significant differences between the surfaces used for the simulations and experiments. Possibly, for normal collisions, a perfectly flat diamond {111} surface transfers substantially more energy to the projectile's vibrational modes than does a rough and partially graphitic surface. As discussed above, energy-transfer to ΔE_{int} is not strongly affected by θ_i for collisions with hydrocarbon molecule and SAM surfaces as a result of their corrugation and roughness.

Possibly the simulations for gly_8-H^+ + diamond {111}, with θ_i = 45° and a percentage energy-transfer to ΔE_{int} of 25% compared with the experimental 19.2%, are more representative of collisions with a rough "diamond-like" surface. However, it should be noted that the percentage energy-transfer to ΔE_{int}, for des-Arg^1-bradykinin, is unaffected by varying the roughness of the "diamond-like" surface [45]. However, the smoothest experimental surface still has a 32 Å roughness.

In future work, it will be important to simulate collisions of des-Arg^1-bradykinin with diamond {111} and compare with the current results for gly_8-H^+. Performing this simulation will require developing an intermolecular potential for the atoms of des-Arg^1-bradykinin interacting with the diamond {111} surface [17, 25]. It will also be of interest to simulate collisions with a graphite surface and compare the results with those presented here for the diamond {111} surface. The results of such a study should provide insight into the different energy-transfer efficiencies found between the perfectly flat diamond {111} surface used in the simulations and the rough, partly graphitic diamond-like surface used in the experiments. Finally, it would be of interest to perform the experiments at θ_i different than 0° (e.g., 45°) to see if the energy-transfer efficiency to ΔE_{int} depends on θ_i for collisions with the rough, diamond-like surface.

Summary

A QM + MM direct dynamics simulation was performed to study energy-transfer and fragmentation in collisions of the protonated octapeptide gly_8-H^+ with the diamond {111} surface, at an initial collision energy E_i of 100 eV and incident angle θ_i of 0° and 45°. Molecular mechanical (MM) functions were used for the gly_8-H^+/diamond intermolecular potential and the potential of the diamond surface. Fragmentation of gly_8-H^+ was studied by representing its intramolecular potential by the AM1 semiempirical quantum mechanical (QM) model.

For θ_i = 0°, the average percentage energy transfers to the internal degrees of freedom of the ion and the surface, and the energy remaining in ion translation, (i.e., ΔE_{int}, ΔE_{surf}, and E_f) are 45%, 26%, and 29%. For the other incident angle studied, 45°, these percentages are 26%, 12%, and 62%. The strong dependence of the energy-transfer to ΔE_{int}, on the incident angle, has not been observed previously in either experimental [40–42] or computational [38] studies of protonated peptide ion collisions with hydrocarbon molecule and self-assembled monolayer (SAM) surfaces. For a smooth and rigid surface, there are no mechanisms for interconverting the normal and parallel components of the incident velocity and, as a result, the energy-transfer dynamics depends only on the normal component with the parallel component conserved [47]. For such systems the energy-transfer scales with $E_i\cos^2\theta_i$. This scale factor changes from 1.0 to 0.5 when θ_i is changed from 0° to 45°, and this is the approximate change in the energy-transfer efficiencies found from the simulations.

The percentage energy-transfer to ΔE_{int} for θ_i = 0° is larger than that reported in previous experiments for collisions of des-Arg^1-bradykinin with a diamond surface at the same θ_i. This difference is discussed in terms of differences between the perfectly flat model diamond {111} surface used in the simulations and the "rough", partially graphitic diamond surface [45, 46] prepared for the experiments.

Shattering dominates gly_8-H^+ fragmentation at θ_i = 0°, with 78% of the ions dissociating in this way. At θ_i = 45° shattering is much less important, but 22% of the colliding ions still shatter. Shattering involves many different fragmentation pathways and for θ_i = 0° there are 304 different pathways, many related by their backbone cleavage patterns. Most of the backbone cleavages occurred via shattering for both incident angles. For the θ_i = 0° fragmentations, 59% resulted from both a-x and b-y cleavages, while for θ_i = 45° 75% of the fragmentations occurred with only a-x cleavage. The high probability of multiple backbone cleavages at θ_i = 0°, compared with 45°, is consistent with the much larger number of fragments formed for the dissociating trajectories for the former angle.

Finally, this work illustrates the utility and importance of using direct dynamics simulations to study the atomic-level dynamics of SID. In the future, it will be of interest to study additional ions, e.g., des-Arg^1-bradykinin, and surfaces.

Acknowledgments

The authors acknowledge that the research reported here is based on work supported by the National Science Foundation under grant no. CHE-0615321 and the Robert A. Welch Foundation under grant no. D-0005. W.L.H. acknowledges important conversations with Julia Laskin and Jean Futrell concerning SID.

References

1. Mabud, M. A.; Dekrey, M. J.; Cooks, R. G. Surface-Induced Dissociation of Molecular Ions. *Int. J. Mass Spectrom. Ion Processes* **1985,** *67*, 285–294.
2. Pradeep, T.; Miller, S. A.; Cooks, R. G. Surface-Induced Dissociation from a Liquid Surface. *J. Am. Soc. Mass Spectrom.* **1993,** *4*, 769–773.
3. Morris, M. R.; Riederer, D. E.; Winger, B. E.; Cooks, R. G.; Ast, T.; Chidsey, C. E. D. Ion/Surface Collisions at Functionalized Self-Assembled Monolayer Surfaces. *Int. J. Mass Spectrom. Ion Processes* **1992,** *122*, 181–217.
4. Håkansson, K.; Axelsson, J.; Palmblad, M.; Håkansson, P. Mechanistic Studies of Multipole Storage Assisted Dissociation. *J. Am. Soc. Mass Spectrom.* **2000,** *11*, 210–217.
5. Wainhaus, S. B.; Lim, H.; Schultz, D. G.; Hanley, L. Energy Transfer and Surface-Induced Dissociation for $SiMe_3^+$: Scattering off clean and Adsorbate Covered Metals. *J. Chem. Phys.* **1997,** *106*, 10329–10336.
6. Meroueh, S. O.; Wang, Y.; Hase, W. L. Direct Dynamics. Simulations of Collision- and Surface-Induced Dissociation of *N*-Protonated Glycine: Shattering Fragmentation. *J. Phys. Chem. A* **2002,** *106*, 9983–9992.
7. Baer, T.; Hase, W. L. *Unimolecular Reaction Dynamics: Theory and Experiments*; Oxford University Press: New York 1996; p 171.
8. Song, K.; Meroueh, O.; Hase, W. L. Dynamics of $Cr(CO)_6^+$ Collisions with Hydrogenated Surfaces. *J. Chem. Phys.* **2003,** *118*, 2893–2902.
9. Wang, Y.; Hase, W. L.; Song, K. Direct Dynamics. Study of *N*-Protonated Diglycine Surface-Induced Dissociation: Influence of Collision Energy. *J. Am. Soc. Mass Spectrom.* **2003,** *14*, 1402–1412.
10. Park, K.; Song, K.; Hase, W. L. An Ab Initio Direct Dynamics Simulation of Protonated Glycine Surface-Induced Dissociation. *Int. J. Mass Spectrom.* **2007,** *265*, 326–336.

11. Laskin, J.; Bailey, T. H.; Futrell, J. H. Shattering of Peptide Ions on Self-Assembled Monolayer Surfaces. *J. Am. Chem. Soc.* **2003,** *125*, 1625–1632.
12. Laskin, J.; Futrell, J. H. Surface-Induced Dissociation of Peptide Ions: Kinetics and Dynamics. *J. Am. Soc. Mass Spectrom.* **2003,** *14*, 1340–1347.
13. Laskin, J.; Futrell, J. H. Collisional Activation of Peptide Ions in FT-ICR Mass Spectrometry. *Mass Spectrom. Rev.* **2003,** *22*, 158–181.
14. Rahaman, A.; Hase, W. L.; Song, K.; Wang, J.; Meroueh, S. Chemical Dynamics Simulations of Energy Transfer and Unimolecular Decomposition in Collision-Induced Dissociation (CID) and Surface-Induced Dissociation (SID). In: *Principles of Mass Spectrometry Applied to Biomolecules*, Laskin, J.; Lifshitz, C., Eds.; Wiley: Hoboken, NJ, 2006; p 379.
15. Laskin, J.; Denisov, E.; Futrell, J. A Comparative Study of Collision-Induced and Surface-Induced Dissociation: 1. Fragmentation of Protonated Dialanine. *J. Am. Chem. Soc.* **2000,** *122*, 9703–9714.
16. Laskin, J.; Futrell, J. H. Energy Transfer in Collisions of Peptide Ions with Surfaces. *J. Chem. Phys.* **2003,** *119*, 3413–3420.
17. Meroueh, O.; Hase, W. L. Dynamics of Energy Transfer in Peptide-Surface Collisions. *J. Am. Chem. Soc.* **2002,** *124*, 1524–1531.
18. Wang, J.; Meroueh, S. O.; Wang, Y.; Hase, W. L. Efficiency of Energy Transfer in Protonated Diglycine and Dialanine SID: Effects of Collision Angle, Peptide Ion Size, and Intramolecular Potential. *Int. J. Mass Spectrom.* **2003,** *230*, 57–63.
19. Bolton, K.; Hase, W. L.; Peslherbe, G. Direct Dynamics Simulations of Reactive System. In: *Modern Methods for Multidimensional Dynamics Computations in Chemistry*, Thompson, D. L. Ed.; World Scientific: London, 1998; p 143–189.
20. Sun, L.; Hase, W. L. Born-Oppenheimer Direct Dynamics Classical Trajectory Simulations. *Rev. Comp. Chem.* **2003,** *19*, 79–146.
21. Cornell, W. D.; Cieplak, P.; Bayly, C. I.; Gould, I. R.; Merz, K. M.; Ferguson, D. M.; Spellmeyer, D. C.; Fox, T.; Caldwell, J. W.; Kollman, P. A. A Second Generation Force Field for the Simulation of Proteins, Nucleic Acids, and Organic Molecules. *J. Am. Chem. Soc.* **1995,** *117*, 5179–5197.
22. Hass, K. C.; Tamor, M. A.; Anthony, T. R.; Banholzer, W. F. Lattice Dynamics and Raman Spectra of Isotopically Mixed Diamond. *Phys. Rev. B* **1992,** *45*, 7171–7182.
23. Miller, S. A.; Luo, H.; Pachuta, S. J.; Cooks, R. G. Soft-Landing of Polyatomic Ions at Fluorinated Self-Assembled Monolayer Surfaces. *Science* **1997,** *275*, 1447–1450.
24. Laskin, J.; Wang, P.; Hadjar, O. Soft-Landing of Peptide Ions onto Self-Assembled Monolayer Surfaces: An Overview. *Phys. Chem., Chem. Phys.* **2008,** *10*, 1079–1090.
25. Deb, B.; Hu, W.; Song, K.; Hase, W. L. An Analytical Potential Energy Function to Model Protonated Peptide Soft-Landing Experiments. The $CH_3NH_3^+/CH_4$ Interactions. *Phys. Chem., Chem. Phys.* **2008,** *10*, 4565–4572.
26. Hase, W. L.; Duchovic, R. J.; Hu, X.; Komornicki, A.; Lim, K. F.; Lu, D. –h; Peslherbe, G. H.; Swamy, K. N.; Vande Linde, S. R.; Varandas, A.; Wang, H.; Wolf, R. J. VENUS: A General Chemical Dynamics Computer Program. *Quantum Chemistry Program Exchange (QCPE) Bulletin.* **1996,** *16*, 671.
27. Frisch, M. J.; Trucks, G. W.; Schlegel, H. B.; Scuseria, G. E.; Robb, M. A.; Cheeseman, J. R.; Montgomery, Jr., J. A.; Vreven, T.; Kudin, K. N.; Burant, J. C.; Millam, J. M.; Iyengar, S. S.; Tomasi, J.; Barone, V.; Mennucci, B.; Cossi, M.; Scalmani, G.; Rega, N.; Petersson, G. A.; Nakatsuji, H.; Hada, M.; Ehara, M.; Toyota, K.; Fukuda, R.; Hasegawa, J.; Ishida, M.; Nakajima, T.; Honda, Y.; Kitao, O.; Nakai, H.; Klene, M.; Li, X.; Knox, J. E.; Hratchian, H. P.; Cross, J. B.; Bakken, V.; Adamo, C.; Jaramillo, J.; Gomperts, R.; Stratmann, R. E.; Yazyev, O.; Austin, A. J.; Cammi, R.; Pomelli, C.; Ochterski, J. W.; Ayala, P. Y.; Morokuma, K.; Voth, G. A.; Salvador, P.; Dannenberg, J. J.; Zakrzewski, V. G.; Dapprich, S.; Daniels, A. D.; Strain, M. C.; Farkas, O.; Malick, D. K.; Rabuck, A. D.; Raghavachari, K.; Foresman, J. B.; Ortiz, J. V.; Cui, Q.; Baboul, A. G.; Clifford, S.; Cioslowski, J.; Stefanov, B. B.; Liu, G.; Liashenko, A.; Piskorz, P.; Komaromi, I.; Martin, R. L.; Fox, D. J.; Keith, T.; Al-Laham, M. A.; Peng, C. Y.; Nanayakkara, A.; Challacombe, M.; Gill, P. M. W.; Johnson, B.; Chen, W.; Wong, M. W.; Gonzalez, C.; and Pople, J. A. *Gaussian 03 Revision D 01*; Gaussian, Inc.: Wallingford CT, 2004.
28. Allinger, N. L. Conformational Analysis. 130. MM2. A Hydrocarbon Force Field Utilizing V1 and V2 Torsional Terms. *J. Am. Chem. Soc.* **1977,** *99*, 8127–8134.
29. Peslherebe, G. H.; Wang, H.; Hase, W. L. Monte Carlo. Sampling for Classical Trajectory Simulations. *Adv. Chem. Phys.* **1999,** *105*, 171–201.
30. Meroueh, O.; Hase, W. L. Effect of Surface Stiffness on the Efficiency of Surface-Induced Dissociation. *Phys. Chem. Chem. Phys.* **2001,** *2*, 2306–2314.
31. Allen, M. P.; Tildesley, D. J. *Computer Simulation of Liquids*; Clarendon: Oxford, 1987; p 228.
32. Schlier, C.; Seiter, A. High-Order Symplectic Integration: An Assessment. *Comput. Phys. Commun.* **2000,** *130*, 176–189.
33. Papayannopoulos, I. A. The Interpretation of Collision-Induced Dissociation Tandem Mass Spectra of Peptides. *Mass Spectrom. Rev.* **1995,** *14*, 49–73.
34. Wysocki, V. H.; Cheng, G.; Zhang, Q.; Hermann, K. S.; Beardsley, R. L.; Hilderbrand, A. E. Peptide Fragmentation Overview. In: *Principles of Mass Spectrometry Applied to Biomolecules*, Laskin, J.; Lifshitz, C., Eds. Wiley: Hoboken, NJ, 2006, p 279.
35. Vachet, R. W.; Bishop, B. M.; Erickson, B. W.; Glish, G. L. Novel Peptide. Dissociation: Gas-Phase Intramolecular Rearrangement of Internal Amino Acid Residues. *J. Am. Chem. Soc.* **1997,** *119*, 5481–5488.
36. Farrugia, J. M.; O'Hair, R. A. J. Involvement of Salt Bridges in a Novel Gas Phase Rearrangement of Protonated Arginine-Containing Dipeptides which Precedes Fragmentation. *Int. J. Mass Spectrom.* **2003,** *222*, 229–242.
37. Yagüe, J.; Paradela, A.; Ramos, M.; Ogueta, S.; Marina, A.; Barahona, F.; López. de Castro, J. A.; Vázquez, J. Peptide Rearrangement during Quadrupole Ion Trap Fragmentation: Added Complexity to MS/MS Spectra. *Anal. Chem.* **2003,** *75*, 1524–1535.
38. Yang, L.; Mazyar, O. A.; Lourderaj, U.; Wang, J.; Rodgers, M. T.; Martínez-Núnez, E.; Addepalli, S. V.; Hase, W. L. Chemical Dynamics Simulations of Energy Transfer in Collisions of Protonated Peptide-Ions with a Perfluorinated Alkylthiol Self-Assembled Monolayer Surface. *J. Phys. Chem. C* **2008,** *112*, 9377.
39. Rahaman, A.; Zhou, J. B.; Hase, W. L. Effects of Projectile Orientation and Surface Impact Site on the Efficiency of Projectile Excitation in Surface-Induced Dissociation: Protonated Diglycine Collisions with Diamond {1 1 1}. *Int. J. Mass Spectrom.* **2006,** *249–250*, 321.
40. Kubišta, J.; Dolejšek, Z.; Herman, Z. Energy Partitioning in Collisions of Slow Polyatomic Ions with Surfaces: Ethanol Molecular Ions on Stainless Steel Surfaces. *Eur. Mass Spectrom.* **1998,** *4*, 311–319.
41. Žabka, J.; Dolejšek, Z.; Herman, Z. Energy Partitioning in Collisions of Slow Polyatomic Ions with Surfaces: Ethanol Molecular Ions on Surfaces Covered by Self-Assembled Monolayers (CF-SAM, CH-SAM, COOH-SAM). *J. Phys. Chem. A* **2002,** *106*, 10861–10869.
42. Herman, Z. Collisions of Slow Polyatomic Ions with Surfaces: The Scattering Method and Results. *J. Am. Soc. Mass Spectrom.* **2003,** *14*, 1360–1372.
43. Tully, J. C. Washboard Model of Gas–Surface Scattering. *J. Chem. Phys.* **1990,** *92*, 680–686.
44. Yan, T.-Y.; Hase, W. L.; Tully, J. C. A Washboard with Moment of Inertia Model of Gas-Surface Scattering. *J. Chem. Phys.* **2004,** *120*, 1031–1043.
45. Yang, Z.; Hadjar, O.; Laskin, J. Effect of the Surface Morphology on the Energy Transfer in Ion–Surface Collisions. *Int. J. Mass Spectrom.* **2007,** *265*, 124–129.
46. Dismukes, J. P.; Ravi, K. V. *Proceedings of the Third International Symposium on Diamond Materials, Electrochemical Society, Pennington*; Honolulu, Hawaii, NJ; May 1993.
47. Goodman, F. O.; Wachman, H. Y. Dynamics of Gas-Surface Scattering; Academic Press: New York, 1976; p 108.